Available online at www.sciencedirect.com

SciVerse ScienceDirect

Journal of the European Ceramic Society 32 (2012) 1585–1591

www.elsevier.com/locate/jeurceramsoc

# Reactive sintering of $U_{1-y}Am_yO_{2\pm x}$ in overstoichiometric conditions

D. Prieur [a,e], F. Lebreton [a], P.M. Martin [b], A. Jankowiak [c], T. Delahaye [a,*], P. Dehaudt [d], P. Blanchart [e]

[a] CEA, DEN/DTEC/SDTC/LEMA, F-30207 Bagnols-sur-Cèze Cedex, France
[b] CEA, DEN/DEC/SESC, F-13108 Saint Paul Lez Durance Cedex, France
[c] CEA, DEN/DANS/DMN/SRMA/LC2M, F-91190 Gif-sur-Yvette, France
[d] CEA, DEN, DTEC/SDTC/DIR, F-30207 Bagnols-sur-Cèze Cedex, France
[e] GEMH, ENSCI, 87065 Limoges, France

Received 30 September 2011; received in revised form 5 December 2011; accepted 11 December 2011
Available online 18 January 2012

**Abstract**

In the framework of Partitioning & Transmutation (P&T), $U_{1-y}Am_yO_{2\pm x}$ materials are promising fuels for Am recycling. In this context, these materials were fabricated in the ATALANTE facility by a process which consists of pelletizing and reactive sintering. Since it was effective in studies conducted on $UO_{2+x}$, sintering in overstoichiometric conditions was investigated. In this work, three Am contents (10, 20 and 30%) and four temperatures (from 1000 to 1300 °C) were studied. It was shown that low-density and multiphasic compounds were obtained. Moreover, XRD and XAFS analyses pointed out that the total reduction of Am(+IV) to Am(+III) and solid solution formation occur during sintering at temperatures inferior to 1300 °C. Although previous studies on $UO_{2+x}$ showed that high oxygen potential enhanced the diffusion process, this work proved that this effect is clearly modified by the presence of Am. Finally, sintering in overstoichiometric conditions is not yet suitable for Am-bearing fuel fabrication.


*Keywords:* Americium; $UO_2$; Sintering; X-ray methods; Nuclear applications

## 1. Introduction

Fissions occurring during fuel irradiation in nuclear reactor lead to the formation of Fission Products (FP), but also, by neutron capture, of Minor Actinides (MA). The latter, which mainly include neptunium (237) and americium (241, 243), are major contributors to spent fuel radiotoxicity. Radioactive waste management research on these long-lived heavy elements is notably directed towards Partitioning and Transmutation (P&T) in Fast Neutron Reactors (FNR) or Accelerator Driven Systems (ADS).[1] For FNR, two recycling modes are generally considered: homogeneous and heterogeneous transmutation. In the first case, MA are added in small quantities (less than 5 wt%) in the fuel[2] whereas in the second case, dedicated fuels, known as blanket fuels, include larger amounts of MA (from 7 to 30 wt%) and are positioned in the core periphery.[3–5] Such a configuration presents a limited impact on the core neutronic behavior. In this context, $U_{1-y}Am_yO_{2\pm x}$ ($y = 0.10$; 0.15; 0.20) oxide solid solutions are increasingly studied as promising blanket fuels for Am recycling in FNR. However, the fabrication of Am-bearing materials requires special attention due both to high $\alpha$ and $\gamma$ activities of Am and its specific thermodynamic properties. Indeed, as shown in Fig. 1, Am oxides exhibit high oxygen potential compared to other actinide oxides. One of the main associated risks is the Am volatilization which can lead to heterogeneous material and microstructure.

Since high-temperature (∼1700 °C) sintering in reducing conditions is now well-known and industrially deployed for $UO_2$ or MOX fuel fabrication, the same sintering conditions were applied at the laboratory scale to fabricate $U_{1-y}Am_yO_{2\pm x}$ ($y = 0.10; 0.20$) pellets. Prieur et al.[3,6,7] showed that dense (>92% of the Theoretical Density (%TD)) and homogeneous materials were achieved in such reducing conditions. Moreover, it was pointed out that fluorite monophasic compounds were obtained. XAS measurements also showed that the reduction from Am(+IV) to Am(+III) is total in these materials.[8] Nevertheless, these conditions are favorable for $AmO_2$ reduction, which could lead to AmO or Am sublimation.

* Corresponding author.
*E-mail address:* thibaud.delahaye@cea.fr (T. Delahaye).

0955-2219/$ – see front matter © 2012 Elsevier Ltd. All rights reserved.
doi:10.1016/j.jeurceramsoc.2011.12.017

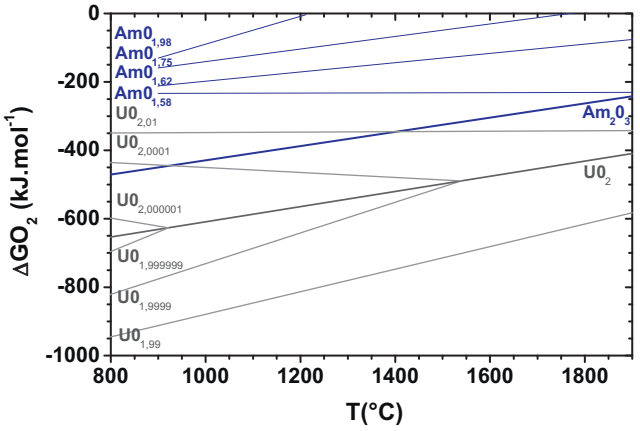


Fig. 1. Oxygen potential $\Delta GO_2$ of both $AmO_{2-x}$ and $UO_{2+x}$ as a function of temperature $T$.

Another sintering method, at lower temperature in overstoichiometric conditions (*i.e.* neutral or oxidizing atmosphere), efficiently produces high-density $UO_{2+x}$ pellets. However, these sintering conditions were only partially explored due to technological reasons. In particular, Williams et al. showed that $UO_2$ pellets sintered under $CO_2$ at 1100 °C had higher densities than same samples sintered at 1700 °C under dry hydrogen.[9] Since this study, several experiments were performed leading to conclude that grain boundary diffusion controls both the first and second stage of $UO_2$ sintering.[10] Such sintering conditions were never tested for $U_{1-y}Am_yO_{2\pm x}$ reactive sintering. Nevertheless, the use of a neutral or oxidizing atmosphere and relatively low temperatures is expected to limit $AmO_2$ reduction and thus Am or AmO sublimation.

In the framework of heterogeneous MA transmutation, this work aims to study the transposition of these overstoichiometric sintering conditions to reactive sintering of U-Am mixed oxide compounds.

## 2. Experimental

### 2.1. Pellet fabrication

$U_{1-y}Am_yO_{2-x}$ ($y = 0.10$; 0.20; 0.30) compounds were fabricated using a conventional powder metallurgy process in the ATALANTE hot cells according to the flow chart given in Fig. 2.[3,11] Both $UO_2$ and $AmO_2$ powders were ball-milled for 30 min at 15 Hz using a Retsch MM200. Additional $UO_2$ powder was then added to adjust the composition and an identical ball-milling step was carried out. Green pellets were uniaxially pressed at 450 MPa using a three-part matrix die. To study the effects of Am content as a function of temperature, samples were sintered 4 h at $T_{sintering} = 1000$, 1100, 1200 and 1300 °C, using a heating rate of 120 °C $h^{-1}$ and a cooling rate of 180 °C $h^{-1}$. During these reactive sinterings, the furnace chamber was maintained under a controlled atmosphere of Ar gas (0.35 ppm $O_2$), for an oxygen potential ranging from −210 to −170 kJ $mol^{-1}$ as a function of temperature (Table 1).

Table 1
Oxygen potential corresponding to the four sintering temperatures.

| $T$ (°C) | 1000 | 1100 | 1200 | 1300 |
|---|---|---|---|---|
| $\Delta GO_2$ (kJ $mol^{-1}$) | −155 (5) | −170 (5) | −180 (5) | −195 (5) |

### 2.2. Pellet characterization

Accurate diameter measurements (accuracy = 2 μm; repeatability = 0.5 μm) were performed on green and sintered samples with a laser micrometer. This equipment is coupled with a step motor to perform regular diameter measurements each 16 μm along the pellet. According to this principle, the pellet is scanned and about 300 diameter measurements are obtained. From these measurements, pellet profiles and geometrical densities were deduced.

Optical microscopy was performed on as-polished samples using an OLYMPUS BX30M microscope.

XRD analyses were carried out using a Bruker D8 Advance diffractometer operating in Bragg-Brentano reflection geometry with Mo($K_{\alpha 1}$) radiation especially equipped for radioactive material measurements. An internal standard (Au) was added to the powdered samples for $2\theta$ calibration of the XRD peak position. The FULLPROF program[12] was used for lattice parameter refinement.

XAS measurements were carried out at the Rossendorf beam line (BM20) of the European Synchrotron Radiation Facility (Grenoble, France). For each sample, fluorescence and transmission signals were collected at the U $L_{II}$, U $L_{III}$ and Am $L_{III}$ edges. Energy calibrations were achieved using Y, Mo and Zr foil located after the second ionization chamber. All measurements were performed at 20 K using a closed-cycle helium cryostat. $E_0$ values and white line positions were respectively taken at

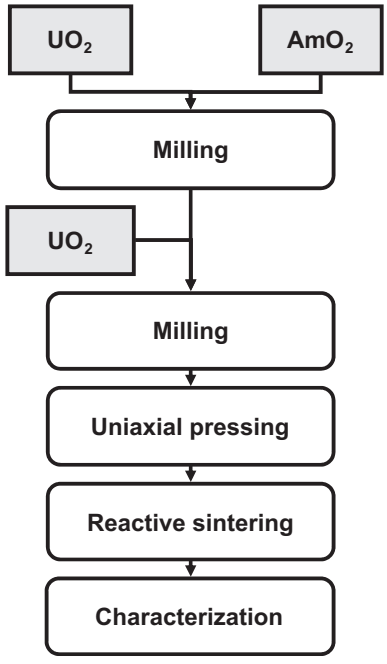


Fig. 2. $U_{1-y}Am_yO_{2\pm x}$ pellet fabrication flow chart.

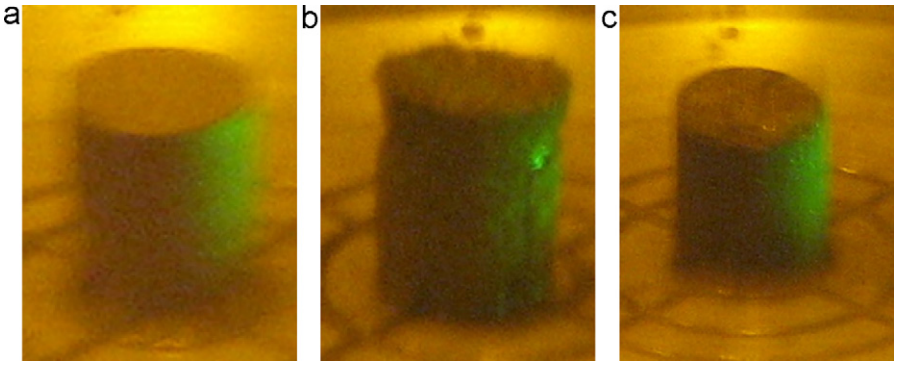


Fig. 3. Photographs of pellets (a) $U_{0.90}Am_{0.10}O_{2\pm x}$, (b) $U_{0.80}Am_{0.20}O_{2\pm x}$ and (c) $U_{0.70}Am_{0.30}O_{2\pm x}$ after sintering at 1300 °C.

the first inflection point using the first zero-crossing value of the second derivative and the first zero-crossing of the first derivative. XANES spectra at the $L_{III}$ edge were compared to data collected on reference compounds on BM20 using the same experimental set-up in order to determine oxidation states of U and Am cations. For U, the reference compounds are $UO_{2.00}$ and $U_4O_{9-\delta}$ whose structures were confirmed using both XRD and neutron diffraction.[13] For Am, $Am^{+IV}O_2$[14] and a mixed oxalate $(U_{0.9}{}^{+IV}Am_{0.1}{}^{+III})_2(C_2O_4)_5{\cdot}6H_2O$[15] were used. The ATHENA software[16] was used for extracting EXAFS oscillations from the raw absorption spectra.

## 3. Results and discussion

### 3.1. Pellet deformations and dedensifications

After the reactive sintering step, pellets were submitted to a visual inspection (Fig. 3). No cracks were found in the sintered pellets. The pellet geometric densities were then measured with the above-described laser micrometer and are reported as a function of temperature in Fig. 4. This device was also used to determine the pellet profiles which are presented in Fig. 5.

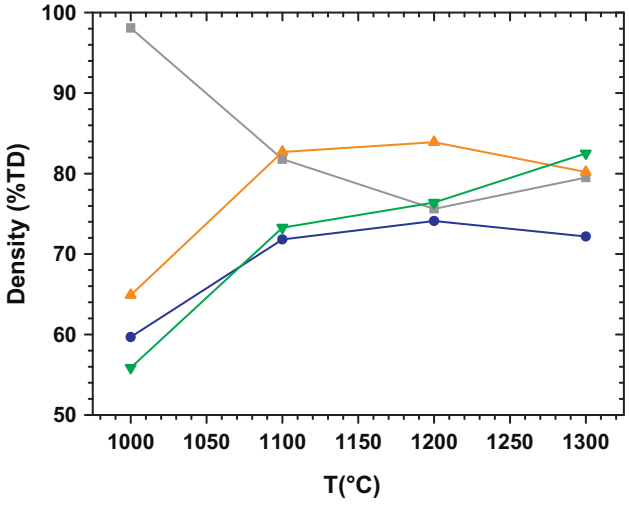


Fig. 4. Sintered densities of pellets containing different amounts of Am (■: $UO_2$; ▲: $U_{0.90}Am_{0.10}O_{2\pm x}$; ●: $U_{0.80}Am_{0.20}O_{2\pm x}$; ▼: $U_{0.70}Am_{0.30}O_{2\pm x}$) as a function of the temperature *T*.

For $UO_2$ materials, sintering at 1000 °C leads to a straight-sided pellet which exhibits a high density: 98.1%TD (Fig. 5(a)). As temperature increases, pellet densities decrease. For both 1100 and 1200 °C, pellets have a hyperboloid-shaped profile whereas an apex-truncated-cone-shaped pellet is achieved for 1300 °C. It can be concluded that $UO_2$ sintering is nearly finished at 1000 °C, whereas a marked decrease in density is observed for higher temperatures, which might be related to pellet dedensification.

Regarding Am-bearing pellets, low geometric densities are achieved, *i.e.* lower than 85%TD. For the materials containing 10 and 20% of Am, maximum values of 83.9%TD and 74.1%TD are respectively reached for sintering at 1200 °C. In the case of the sample containing 30% of Am, the highest density (82.5% TD) is obtained at 1300 °C. Fig. 5(b) and (c) give the pellet profiles for 10 and 20% Am-bearing pellets, which exhibit similar behaviors with temperature. At 1000 °C, little shrinkage is measured and quite straight profiles are observed. For higher temperatures (1200 °C for 10% of Am and 1000 °C for 20% of Am), variations in diameter occur, leading to apex-truncated-cone-shaped pellets. These distortions increase with temperature. As seen in Fig. 5(d), diameter variations are more pronounced in 30% Am samples, but decrease with temperature. Except in the 30% Am samples, it seems that denser pellets cannot be obtained by increasing temperature, as a maximum is reached at 1200 °C. Instead, a dedensification phenomenon is observed for higher temperatures.

Based on these density and profile measurements, it can be concluded that both dedensification and deformation of $UO_2$ and Am-bearing pellets occur during reactive sintering in overstoichiometric conditions. This indicates that these phenomena do not depend either on presence or distribution of Am. Therefore, several assumptions can be made to explain observed dedensification and deformation.

Firstly, the dedensification might result from the presence of residual carbon in the green pellet. This impurity comes from the inorganic lubricant used for uniaxial pressing and from the precursor powders. In contact with oxygen, residual carbon oxidation might occur, leading to $CO_2$ bubbles and porosity formation. This phenomenon, called solarization, is particularly enhanced in these overstoichiometric conditions.[17] Furthermore, the presence of carbon in the powders reduces the O/U ratio, leading to decreased pellet sinterability. Thus,

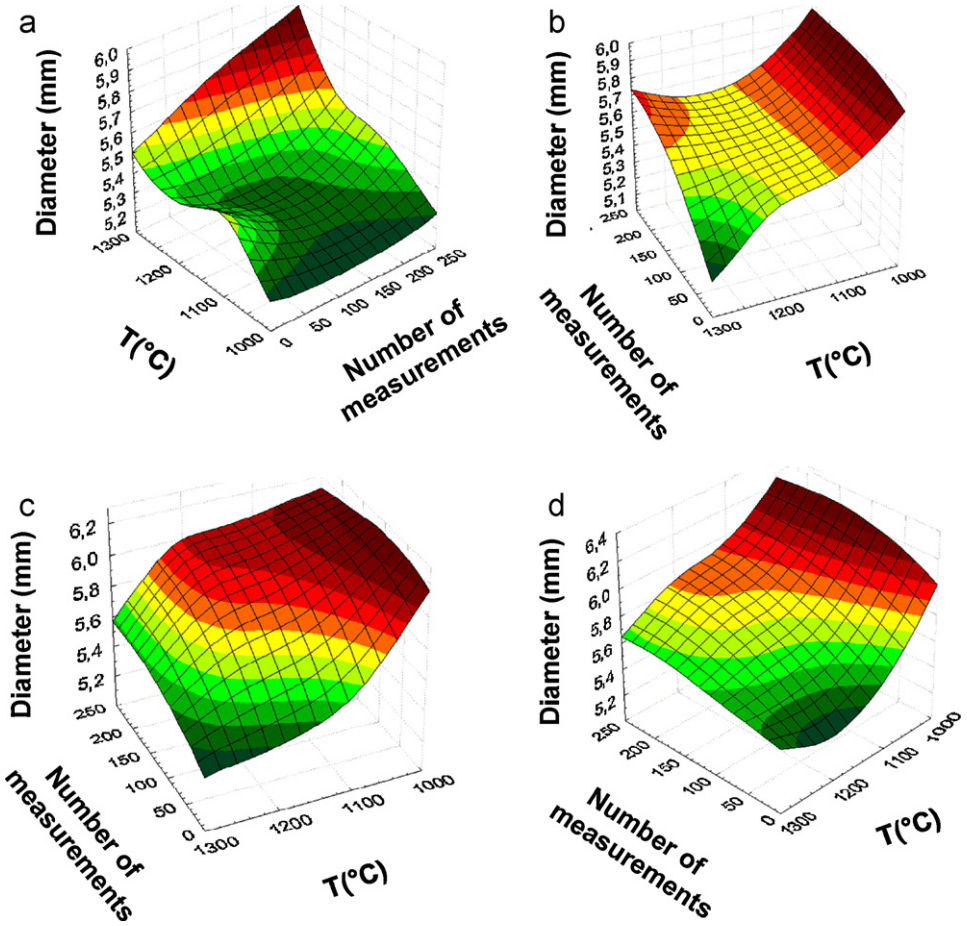


Fig. 5. Profiles after sintering for pellets of (a) $UO_2$, (b) $U_{0.90}Am_{0.10}O_{2\pm x}$, (c) $U_{0.80}Am_{0.20}O_{2\pm x}$ and (d) $U_{0.70}Am_{0.30}O_{2\pm x}$ as a function of the temperature $T$. The number of measurements corresponds to the height of the pellet.

the presence of carbon might explain the difficulty encountered in obtaining higher densities under these sintering conditions. However, in the optical micrographs for pellets containing 10 and 30% of Am (Fig. 6), no spherical pores, characteristic of solarization are observed, which excludes solarization as an explanation for the observed dedensification.

Secondly, another parameter to consider is the sintering atmosphere. Indeed, it plays an important role in the sintering behavior and might explain the observed dedensification phenomenon. Nevertheless, if the atmosphere alone was responsible for pellet deformation, a homogeneous or, at least, a symmetric expansion would be expected. The cone-shaped profiles are probably caused by another parameter which is strongly related to the atmosphere such as the orientation of the pellets in the furnace. Since the bottom face of the pellet is less exposed to the atmosphere than the top face, exchanges with atmosphere are less favored. As incorporation of oxygen into the lattice tends to cause swelling, the pellet deformation in such a configuration would neither be constant nor symmetric. Due to experimental conditions in hot cells, this interpretation is difficult to investigate further.

Finally, the observed density decrease might be explained by the presence of a trivalent cation. It was shown for uranium-lanthanide mixed oxides that in overstoichiometric conditions, incomplete sintering was achieved in presence of a trivalent cation.[18] To confirm this assumption, XANES measurements were performed. The XANES spectra at the U $L_{III}$ and Am $L_{III}$ edges and the corresponding second derivatives are given in Fig. 7. At the Am $L_{III}$ edge, it can be seen that there is no shift in inflection point or white line positions (Fig. 7 and Table 2). It indicates that the Am oxidation state is (+III) despite the high oxygen potential used during sintering ($-210\,kJ\,mol^{-1}$). Regarding the U $L_{III}$ edge, a shift of both inflection point and white line positions toward higher energy is observed, indicating a mixed valence U(+IV/+V). By analogy with uranium-lanthanide mixed oxides, the dedensification of the Am-bearing pellets might be explained by the presence of the trivalent cation Am(+III).

### 3.2. Solid solution formation vs. densification

In the optical micrographs presented in Fig. 6, two phases are clearly visible. The largest corresponds to an $UO_{2+x}$-type phase (white arrow), composed of very large and angular-shaped grains whose mean equivalent diameter is estimated at 40 μm. Surrounding these grains, a darker grey Am-rich second phase is observed. The multiphasic character of the compound is consistent with XRD analyses performed on samples sintered at 1300 °C, containing 10 and 30% of Am. As shown in Fig. 8,

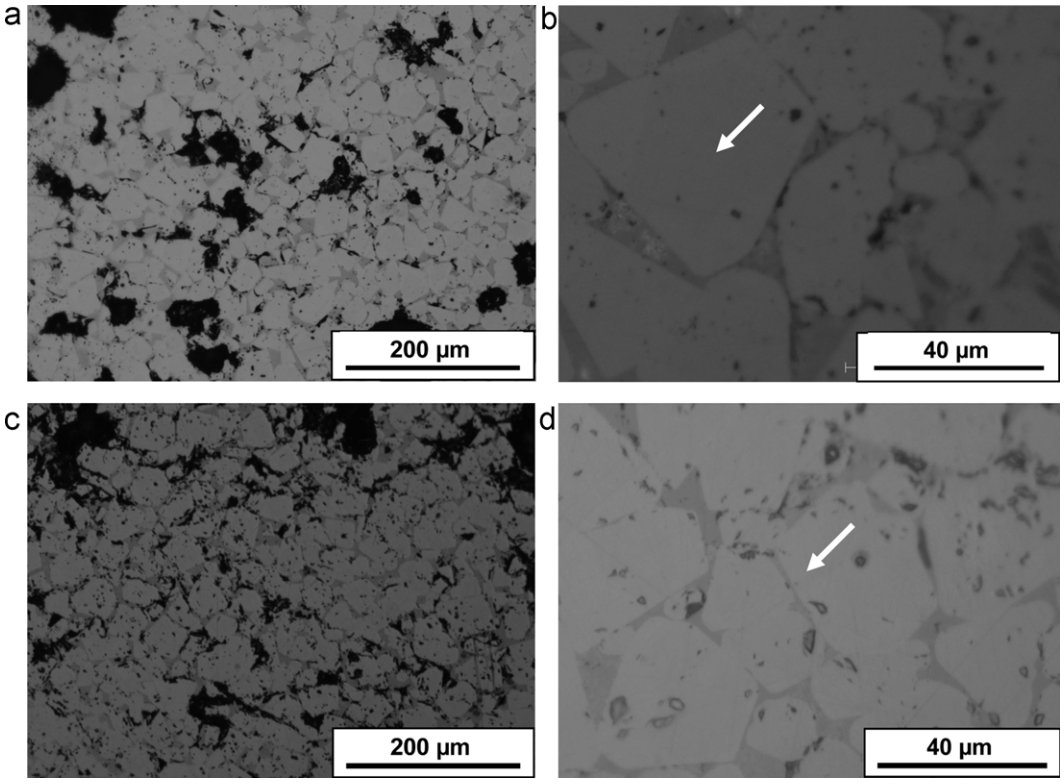


Fig. 6. Optical micrographs of mirror-polished samples $U_{0.90}Am_{0.10}O_{2\pm x}$ and $U_{0.70}Am_{0.30}O_{2\pm x}$ sintered at 1300 °C ($U_{0.90}Am_{0.10}O_{2\pm x}$ (a): ×10 and (b): ×50; $U_{0.70}Am_{0.30}O_{2\pm x}$ (c): ×10 and (d): ×50).

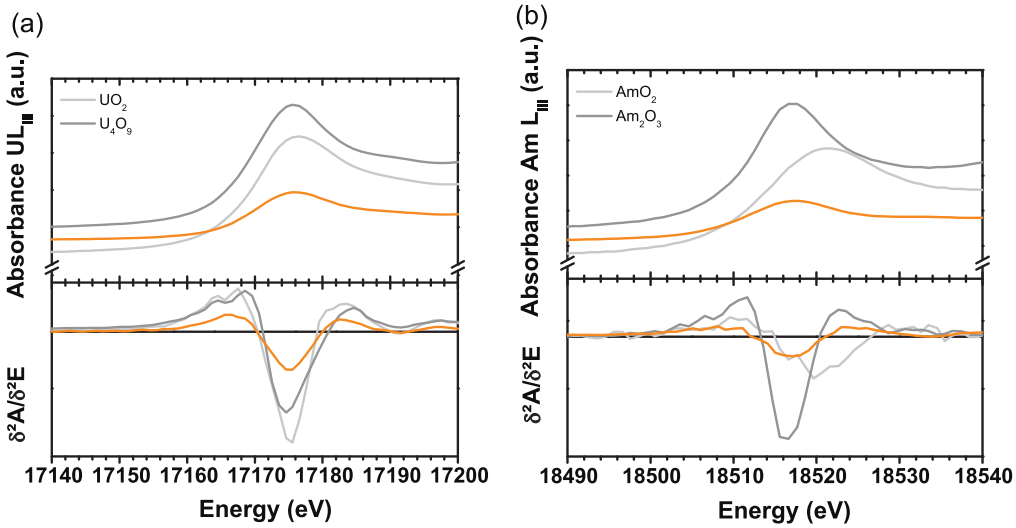


Fig. 7. XANES spectra and second derivatives of (—) $U_{0.90}Am_{0.10}O_{2\pm x}$ at U $L_{III}$ (a) and Am $L_{III}$ (b) edges.

Table 2
Position of the white line and inflection points of the XANES spectra.

| Sample | Composition | Am $L_{III}$ edge | | U $L_{III}$ edge | |
|---|---|---|---|---|---|
| | | Inflection point (eV) | White line (eV) | Inflection point (eV) | White line (eV) |
| Studied sample | $U_{0.90}Am_{0.10}O_{2\pm x}$ | 18512.1 | 18517.7 | 17170.3 | 17175.6 |
| Reference compound | $UO_2$ | | | 17169.7 | 17175.6 |
| Reference compound | $UO_{2.25}$ | | | 17170.8 | 17175.4 |
| Reference compound | $Am^{+IV}O_2$ | 18514.2 | 18521.5 | | |
| Reference compound | $(U_{0.9}{}^{+IV}Am_{0.1}{}^{+III})_2(C_2O_4)_5{\cdot}6H_2O$ | 18512.4 | 18517.7 | | |

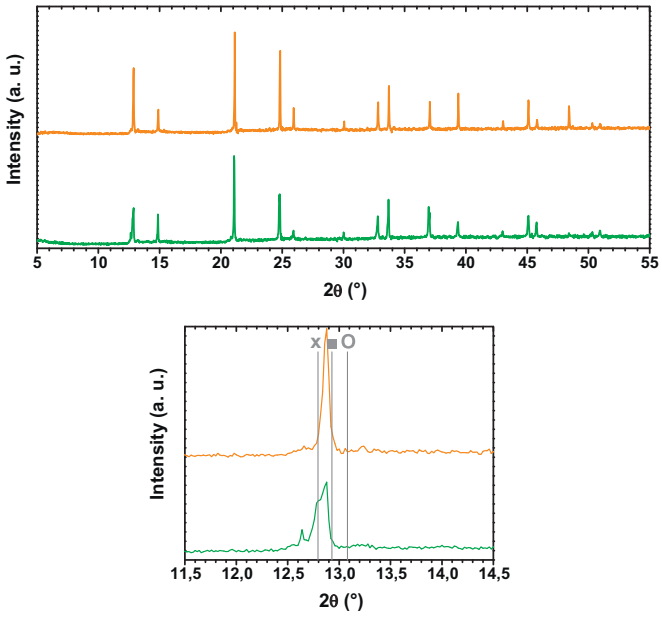


Fig. 8. X-ray diffraction patterns of two samples sintered at 1300 °C: (_) $U_{0.90}Am_{0.10}O_{2\pm x}$ and (_) $U_{0.70}Am_{0.30}O_{2\pm x}$ from 5 to 55° and from 11.5 to 14.5° (X: $Am_2O_3$; ■: $UO_{2.16}$; ◯: $AmO_2$).

Table 3
Lattice parameters of phases determined for $U_{0.90}Am_{0.10}O_{2\pm x}$.

| Phase | Space group | Lattice parameter (Å) | R-Bragg | $\chi^2$ |
|---|---|---|---|---|
| Preponderant fluorine | F m-3m | 5.467 (1) | 2.62 | 3.12 |
| Low level fluorine | F m-3m | 5.541 (1) | 3.21 | 4.68 |
| $UO_{2+x}$ | F m-3m | 5.468 (1) | 2.89 | 3.47 |

XRD patterns indicate that three phases with fluorite structures, one being $UO_{2+x}$, are found for both samples. Concerning the remaining two phases, the first one is found to be predominant and the second is the least common. This difference is greater for samples with 30% of Am. After data refinement, lattice parameters were calculated for the phases and are given in Table 3 and Table 4. Since the preponderant phase exhibits a lattice parameter inferior to that of $UO_{2+x}$, this phase might correspond to a $U_yAm_{1-y}O_{2\pm x}$ solid solution which is different from the expected ones. This indicates that the solid solution formation begins below 1300 °C for these sintering conditions.

From the XANES spectra given in Fig. 7, the molar fractions of Am(+III), U(+IV) and U(+V) were determined by linear combination of the reference compounds and are presented in Table 5. These results show that total reduction from Am(+IV) to Am(+III) occurs under 1300 °C, whereas a partial oxidation of U(+IV) to U(+V) is observed for these sintering conditions.

Table 4
Lattice parameters of phases determined for $U_{0.70}Am_{0.30}O_{2\pm x}$.

| Phase | Space group | Lattice parameter (Å) | R-Bragg | $\chi^2$ |
|---|---|---|---|---|
| Preponderant fluorine | F m-3m | 5.466 (1) | 2.79 | 3.48 |
| Low level fluorine | F m-3m | 5.574 (1) | 3.48 | 5.03 |
| $UO_{2+x}$ | F m-3m | 5.468 (1) | 3.01 | 3.72 |

Table 5
Molar fractions of Am(+III), Am(+IV), U(+IV) and U(+V) obtained by fitting XANES results with linear combination of reference compounds $Am_2O_3$, $AmO_2$, $UO_2$ and $U_4O_9$.

| Sintering conditions | Composition | Molar fractions (at.%) | | | |
|---|---|---|---|---|---|
| | | Am(+III) | Am(+IV) | U(+IV) | U(+V) |
| 1300 °C | $U_{0.90}Am_{0.10}O_{2\pm x}$ | 0.10 (2) | 0.00 (2) | 0.81 (2) | 0.09 (2) |

The total reduction of Am is in agreement with the high oxygen potential of Am and the work of Thiriet and Konings on the Am-O system.[19] Given the high oxygen potential, the mixed valence U(+IV/+V) is also an expected result. Moreover, the presence of U(+V) is normal since a $UO_{2+x}$ phase was found via XRD analysis. With regards to the U cations, their mixed valence can be explained by electronic compensation for the overstoichiometric state of $UO_{2+x}$ before solid solution formation. Additional experiments will be required to study this assumption. Nevertheless, according to the total reduction of Am in these conditions, it is shown that Am(+III) diffuses in $UO_{2+x}$. As it remains Am(+III) in the structure, $O_2$ is released, so a decrease of the solid solution stoichiometry is expected.

In addition, the observed $U_yAm_{1-y}O_{2\pm x}$ solid solution is different from the expected one since the Am content is not equal to 15%. This shows that U/Am interdiffusion is insufficient to permit solid solution formation at such low temperatures, which confirms that Am delays densification. These results are consistent with a reactive sintering. During this process, a large quantity of energy is consumed by U/Am interdiffusion and solid solution formation, so sintering will be slowed as long as this solid solution is not completely formed. Though the atmospheric conditions used favor nonstoichiometric states, and consequently better $UO_2$ diffusion and densification,[20] it is understandable that the sintered density was so low, as the $U_{0.85}Am_{0.15}O_{2\pm\delta}$ solid solution was not completely formed.

## 4. Conclusion

The present paper aims to study the sintering behavior of $U_{1-y}Am_yO_{2\pm x}$ in overstoichiometric conditions at low temperature. Since these sintering conditions were developed on $UO_{2\pm x}$ fuel, they were extended to $U_{1-y}Am_yO_{2\pm x}$ reactive sintering. In this context, $U_{1-y}Am_yO_{2\pm x}$ compounds were fabricated in the ATALANTE facility using a pelletizing and sintering process. The pellets were sintered at various temperatures, *i.e.* 1000, 1100, 1200 and 1300 °C. It was shown that low-density and multiphasic materials were obtained. XRD analysis pointed out that solid solution formation begins at a temperature inferior to 1300 °C. Although the high oxygen potential favored both diffusion and densification processes for $UO_{2\pm x}$, it seems that, for $U_{1-y}Am_yO_{2\pm x}$, the solid solution formation consumed a significant part of the available energy. Therefore, densification cannot be achieved, explaining the low observed densities.

Finally, compared to sintering in reducing conditions, sintering in overstoichiometric conditions is not yet suitable for the fabrication of Am-bearing materials.

## Acknowledgements

The authors are grateful to N. Astier, M. Bataille and P. Coste for the sample preparation. The authors also acknowledge B. Arab-Chapelet and R. Belin for respectively providing the XAS spectra of $AmO_2$ and oxalate reference compounds. D. Prieur, F. Lebreton and T. Delahaye would like to specially thank N. Reilly for her sensitive advice. The authors thank the European Synchrotron Radiation Facility for provision of synchrotron radiation facilities.

## References

1. Warin D. Status of the French research program on partitioning and transmutation. *Journal of Nuclear Science and Technology* 2007;**44**: 410–4.
2. Lebreton F, Prieur D, Jankowiak A, Delahaye T, Tribet M, Donnet L, et al. Fabrication and characterization of americium, neptunium and curium bearing MOX fuels obtained by powder metallurgy process. *Journal of Nuclear Materials* 2011;**420**:213–7.
3. Prieur D, Jankowiak A, Delahaye T, Herlet N, Dehaudt P, Blanchard P. Fabrication and characterisation of $U_{0.85}Am_{0.15}O_{2-x}$ for MARIOS irradiation program. *Journal of Nuclear Materials* 2011;**414**:503–7.
4. Grouiller JP, Pillon S, de Saint Jean C, Varaine F, Leyval L, Vambenepe G, et al. Minor actinides transmutation scenario studies with PWRs, FRs and moderated targets. *Journal of Nuclear Materials* 2003;**320**:163–9.
5. Delpech M, Grouiller JP. *NT DER/SPRC/LEDC* 1997:96–462.
6. Prieur D, Jankowiak A, Leorier C, Herlet N, Donnet L, Dehaudt P, et al. Influence of the microstructure of the $U_{1-y}Am_yO_{2-x}$ ($y = 0.1$; 0.15) pellet macroscopic swelling. *Advances in Science and Technology* 2010;**73**: 104–8.
7. Prieur D, Jankowiak A, Roudil D, Dubois S, Leorier C, Herlet N, et al. Self-irradiation effects in dense and tailored porosity $U_{1-y}Am_yO_{2-x}$ ($y = 0.10$; 0.15) compounds. *Journal of Nuclear Materials* 2011;**411**: 15–9.
8. Prieur D, Martin PM, Jankowiak A, Scheinost A, Herlet N, Dehaudt P, et al. Local structure and charge distribution in mixed uranium-americium oxides: effects of oxygen potential and Am content. *Inorganic Chemistry* 2011;**50**:12437–45.
9. Williams J, Barnes E, Scott R, Hall A. Sintering of uranium oxide of composition $UO_2$ to $U_3O_8$ in various atmospheres. *Journal of Nuclear Materials* 1959;**1**:28–38.
10. Chevrel H, Dehaudt P, Francois B, Baumard JF. Influence of surface phenomena during sintering of overstoichiometric uranium dioxide $UO_{2+x}$. *Journal of Nuclear Materials* 1992;**189**:175–82.
11. Prieur D, Jankowiak A, Leorier C, Herlet N, Donnet L, Dehaudt P, et al. Fabrication and characterization of minor actinides bearing fuels obtained by conventional powder metallurgy process. *Powder Technology* 2011;**208**:553–7.
12. Carjaval JR. Satellite meeting on powder diffraction of the XV IUCr Congress; 1990.
13. Desgranges L, Baldinozzi G, Rousseau G, Niepce J, Calvarin G. Neutron diffraction study on the in situ oxidation of $UO_2$. *Inorganic Chemistry* 2009;**48**:7585–92.
14. Belin RC, Martin PM, Valenza PJ, Scheinost AC. Experimental insight into the radiation resistance of zirconia-based americium ceramics. *Inorganic Chemistry* 2009;**48**:5376–81.
15. Grandjean S, Arab-Chapelet B, Robisson AC, Abraham F, Martin Ph, Dancausse JP, et al. Structure of mixed U(IV)-An(III) precursors synthesized by co-conversion methods (where An = Pu, Am or Cm). *Journal of Nuclear Materials* 2009;**385**:204–7.
16. Ravel B, Newville M. ATHANE, ARTEMIS, HEPHAESTUS: data analysis for X-ray absorption spectroscopy using IFEFFIT. *Journal of Synchrotron Radiation* 2005;**12**:537–41.
17. Assmann H, Dorr W, Peehs M. Control of $UO_2$ microstructure by oxidative sintering. *Journal of Nuclear Materials* 1986;**140**:1–6.
18. Rocaniere C. Contribution to the study of the systems uranium oxide – lanthanoide oxide. Ph.D. Thesis, University of Limoges; 1998.
19. Thiriet C, Konings RJM. Chemical thermodynamic representation of $AmO_{2-x}$. *Journal of Nuclear Materials* 2003;**320**:292–8.
20. Matzke H. Point defects and transport properties in carbides. *Solid State Ionics* 1984;**12**:25–45.